Collaboration and competition between active sheets for self-propelled particles

Abhrajit Laskar[a], Oleg E. Shklyaev[a], and Anna C. Balazs[a,1]

[a]Department of Chemical and Petroleum Engineering, University of Pittsburgh, Pittsburgh, PA 15261

Edited by David A. Weitz, Harvard University, Cambridge, MA, and approved April 2, 2019 (received for review January 23, 2019)

Biological species routinely collaborate for their mutual benefit or compete for available resources, thereby displaying dynamic behavior that is challenging to replicate in synthetic systems. Here we use computational modeling to design microscopic, chemically active sheets and self-propelled particles encompassing the appropriate synergistic interactions to exhibit bioinspired feeding, fleeing, and fighting. This design couples two different mechanisms for chemically generating motion in fluid-filled microchambers: solutal buoyancy and diffusiophoresis. Catalyst-coated sheets, which resemble crabs with four distinct claws, convert reactants in solution into products and thereby create local variations in the density and chemical composition of the fluid. Via the solutal buoyancy mechanism, the density variations generate fluid flows, which modify the shape and motility of the crabs. Concomitantly, the chemical variations propel the motion of the particles via diffusiophoresis, and thus, the crabs' and particles' motion becomes highly interconnected. For crabs with restricted lateral mobility, these two mechanisms can be modulated to either drive a crab to catch and appear to feed on all of the particles or enable the particles to flee from this sheet. Moreover, by adjusting the sheet's size and the catalytic coating, two crabs can compete and fight over the motile, diffusiophoretic particles. Alternatively, the crabs can temporally share resources by shuttling the particles back and forth between themselves. With completely mobile sheets, four crabs can collaborate to perform a function that one alone cannot accomplish. These findings provide design rules for creating chemically driven soft robotic sheets that significantly expand the functionality of microfluidic devices.

chemically active sheets | solutal buoyancy | diffusiophoretic particles

Cooperation and competition are fundamental modes of interaction that are critical to the survival of biological organisms. An intriguing question is whether these behaviors are exhibited solely by living systems or can in fact be performed by synthetic objects. Determining the limits to which man-made systems can mimic complex biological interactions is important for designing the next generation of smart devices and robotic systems. On a fundamental level, addressing this question is important for understanding basic biochemical factors that drive collective behavior. Notably, researchers have designed material systems that display lifelike functionality in the presence of external cues. For example, in the presence of an applied magnetic field, magnetic particles appear to hunt and steal beads from other assemblies (1); in the presence of light, photoresponsive particles unite to form complex structures (2). In addition to responding to external stimuli, biological systems can inherently generate chemical cues that prompt neighboring organisms to carry out vital tasks (3). Herein, we use computational modeling to design self-propelled, catalyst-coated sheets that not only generate the fluid flows that drive their own mobility but also produce the chemical gradients that direct the motion of chemoresponsive microparticles in the solution. Researchers have just recently examined the behavior of chemically active sheets immersed in fluids (4), and thus, the rich dynamic interactions that can occur between active sheets and particles have not previously been investigated. As shown below, these interactive sheets and particles exhibit such lifelike attributes as fighting, feeding, and fleeing. Localized in a fluid-filled microchamber, all these behaviors can greatly expand the functionality of microfluidic devices.

The self-propulsion of microscopic particles dispersed in solution can occur through various mechanisms. In the case of diffusiophoresis, particles respond to chemical variations near a surface by moving with a velocity that is proportional to gradients in the local reagent concentration (5). In scenarios involving solutal buoyancy, catalyst-coated particles produce products that have a different density than the initial reactants. The resulting density gradients drive the motion of the bulk fluid, which in turn can drive the particles' motion (6, 7). For rigid particles, this fluid motion does not alter the particle's shape. In contrast to the particles, recent computer simulations revealed that flows generated by catalyst-coated, flexible sheets via solutal buoyancy not only propel but also sculpt the shape of the sheets (4). Hence, chemically active sheets can permit new forms of dynamic and collective behavior. Moreover, these sheets can serve as active components in new types of chemically driven microscale, soft robotic systems.

We take advantage of both the above mechanisms and the distinctive behavior of active, flexible sheets to devise the systems described below. Namely, we harness the chemical gradients in reactants and products produced by the active sheet to drive the movement of the diffusiophoretic particles in the fluid (Fig. 1). Here the motion and shape-changing of the sheets affects the dynamics of both the particles and fluid and can yield new synergistic behavior. To simulate this multicomponent system, we formulate the set of coupled equations described below that

Significance

Chemical and density gradients produced by catalytic reactions provide effective means of propelling particles in fluid-filled microchambers. Using computer modeling, we show the rich dynamic behavior that emerges when catalyst-coated sheets are combined with chemoresponsive particles in solution. Catalytic reactions on the flexible sheets generate density variations that produce fluid flows, which deform the sheets and drive their movement. The same reactions yield the chemical gradients that direct the particles' motion. The resulting synergistic interactions among the sheets, particles, and fluid lead to bioinspired behavior, such as crab-shaped sheets competitively grabbing or collaboratively sharing particles, which can also flee these predators. By identifying parameters that govern the systems' behavior, we provide guidelines for creating chemically driven, flexible robots for fluidic environments.

Author contributions: A.C.B. designed research; A.L., O.E.S., and A.C.B. performed research; A.L., O.E.S., and A.C.B. contributed new reagents/analytic tools; A.L., O.E.S., and A.C.B. analyzed data; and A.L., O.E.S., and A.C.B. wrote the paper.

The authors declare no conflict of interest.

This article is a PNAS Direct Submission.

[1]To whom correspondence should be addressed. Email: balazs@pitt.edu.

This article contains supporting information online at www.pnas.org/lookup/suppl/doi:10.1073/pnas.1901235116/-/DCSupplemental.

Published online April 24, 2019.

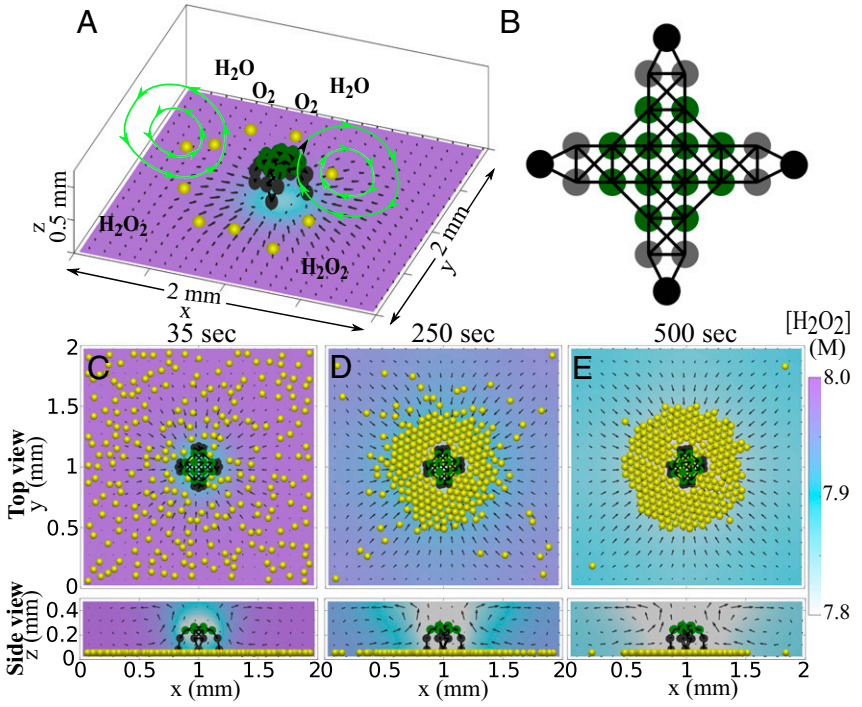

Fig. 1. Components of the system. (*A*) Schematic of the enzyme-coated sheet, which generates the inward flow (outlined in light green), and the diffusiophoretic particles (yellow spheres). (*B*) Within the sheet, the catalase-coated nodes are marked in green, and the heavier nodes at the apexes are indicated in black. (*C–E*) Snapshots from simulations revealing the gradual aggregation of particles around sheet. Black arrows indicate magnitude and direction of fluid velocity. Here $\alpha = 1 \times 10^{-12}\,\mathrm{m^5 mol^{-1} s^{-1}}$ for the particles. Color bar indicates the concentration of H_2O_2 in the solution.

account for the catalytic reactions, fluid dynamics, motion of the particles and sheets, and fluid–structure interactions between the solution and solid surfaces.

Theoretical Model

The fluid-filled microchamber in Fig. 1*A* contains two types of active objects: enzyme-coated elastic sheets and diffusiophoretic particles. The composition of the solution is controlled by reactions catalyzed by enzymes (immobilized on the surface of the sheets), which transform the reactants into products. Due to this reaction, the density of the solution changes because the reactant and product molecules occupy different volumes in the fluid (6). The resulting slight expansion or contraction of the solution is characterized by the solutal expansion coefficient β, which is specific to the particular chemicals and solvents. For sufficiently small concentrations of the reactants and products, the density of the solution can be approximated as $\rho = \rho_0(1 + \sum \beta_j C_j)$, where ρ_0 is the solvent density, C_j is the concentration of the dissolved chemicals, and $\beta_j = \partial\rho/\partial C_j$ are the corresponding expansion coefficients (8, 9). [These density variations are analogous to those due to thermal buoyancy (9), where variations in heat produce the density gradients that produce flow.]

The spatial variations in the solution's density gives rise to the solutal buoyancy force $\mathbf{F}_\mathrm{b} = \mathbf{g}\rho_0 \sum \beta_j C_j$ (directed along the gravity vector $\mathbf{g}$) that drives the motion of the fluid, which, in turn, imposes a fluid drag on objects immersed in the solution. When the products of the chemical reaction are denser (less dense) than the reactants, then the product-rich fluid flows downward to the bottom (upward to the top) of the chamber, and its volume is replaced by the reactant-rich fluid. In a confined chamber, the buoyancy-generated convective flows are circular (as emphasized by green lines in Fig. 1*A*) due to the continuity of the fluid.

N mobile particles (yellow spheres in Fig. 1*A*) with coordinates $\mathbf{r}_i = (x_i, y_i, z_i)$ $(1 \le i \le N)$ are immersed in the solution. A particle of radius a has a density ρ_p and is subject to the gravitational force $\mathbf{F}_\mathrm{g}^\mathrm{p} = 4\pi a^3(\rho_\mathrm{p} - \rho_0)\mathbf{g}/3$ directed along the vector $\mathbf{g}$. Each particle experiences a repulsive interaction with the other particles, elastic sheets, and chamber walls. The respective repulsive forces, $\mathbf{F}^\mathrm{pp}$, $\mathbf{F}^\mathrm{pn}$, and $\mathbf{F}^\mathrm{pw}$, are defined as $\mathbf{F}_\mathrm{r}(r) = -\partial U(r)/\partial \mathbf{r}$, where U is the following Morse potential:

$$U(r) = \begin{cases} \varepsilon(1 - \exp[-\omega\,(r - r_0)])^2, & r < r_0 \\ 0, & r \ge r_0 \end{cases}. \qquad [1]$$

Here $r = |\mathbf{r}_i - \mathbf{r}_x|$ is the distance between the position of the particle $\mathbf{r}_i$ and the repelled object $\mathbf{r}_x$. The parameters ε and ω denote the strength and width of the potential, respectively, and r_0 is the equilibrium (and cutoff) distance.

The diffusiophoretic particles respond to the local chemical variations arising from the enzymatic reactions by spontaneously moving with a velocity

$$\mathbf{u}^\mathrm{ph} = \alpha_j \nabla C_j, \qquad [2]$$

where ∇C_j characterizes the chemical gradients and the constant α_j characterizes the interactions between the molecules of some particular solute j and the adjacent fluid/particle interface (5).

Each enzyme-coated flexible sheet is discretized into a single layer network of M nodes located at $\mathbf{r}_k$ $(1 \le k \le M)$ and interconnected by elastic bonds (4). For the four-lobe sheet in Fig. 1*B*, the spheres and black lines represent the respective discretization nodes and the interconnecting bonds. The elastic forces, $\mathbf{F}_\mathrm{el}$, that arise due to the stretching and bending of bonds connecting the nodes are governed by the linear constitutive relations for a Kirchoff rod (10). The minimum elastic energy is attained when the sheet is in the flat configuration. Each of the sheet's nodes represents a portion of material with volume V, surface area S, and density ρ_n and experiences an external force, $\mathbf{F}_\mathrm{g}^\mathrm{n} = V(\rho_\mathrm{n} - \rho_0)\mathbf{g}$. For the current application, we specify the values of density $\rho_\mathrm{n}(\mathbf{r}_k)$ as a function of the position of the node $\mathbf{r}_k$ within the elastic network. In particular, the nodes at the apex of each lobe (drawn in black in Fig. 1*B*) have a higher density than the other nodes, which makes them less buoyant. Finally, each node of the sheet repels the mobile particles, nodes of other sheets, and walls of the chamber with the forces $\mathbf{F}^\mathrm{np}$, $\mathbf{F}^\mathrm{nn}$, and $\mathbf{F}^\mathrm{nw}$, respectively, defined through the repulsive force $\mathbf{F}_\mathrm{r}$ introduced above.

The chemical reactions in the chamber are catalyzed by M_a chemically active nodes in the sheet (green spheres in Fig. 1*B*). (The gray and black spheres are chemically inactive.) The rate of reaction on the coated sheet is $KS = \frac{r^{\text{enzyme}}_{\text{m, sheet}} C_j}{K_M + C_j} S$ (mol s^{-1}), where K_M is the Michaelis constant and the maximal reaction rate $r^{\text{enzyme}}_{\text{m, sheet}} = k[E]$ (mol s^{-1} m^{-2}) incorporates the reaction rate per molecule of enzyme k and the areal enzyme concentration $[E]$. S is the surface area of sheet's active region.

The behavior of the entire system is described by following equations for the fluid dynamics (Navier–Stokes [in the Boussinesq approximation (11)]) and the continuity of the fluid; the advection, diffusion, and reaction of the dissolved chemical species; and the dynamic behavior of the mobile particles and the nodes of the elastic sheets. The respective equations are

$$\nabla \cdot \mathbf{u} = 0, \qquad [3]$$

$$\frac{\partial \mathbf{u}}{\partial t} + (\mathbf{u} \cdot \nabla)\mathbf{u} = -\frac{1}{\rho_0}\nabla p + \nu\, \nabla^2 \mathbf{u} + \frac{1}{\rho_0}(\mathbf{F}_b + \mathbf{F}_{el}), \qquad [4]$$

$$\frac{\partial C_j}{\partial t} + (\mathbf{u} \cdot \nabla)C_j = D_j \nabla^2 C_j \pm SK \sum_{l=1}^{M_a} \delta(\mathbf{r}_l - \mathbf{r}), \quad 1 \le j \le J, \qquad [5]$$

$$\frac{\partial \mathbf{r}_i}{\partial t} = \mathbf{u}^{\text{ph}} + \mathbf{u} + \mu\left(\mathbf{F}^{\text{p}}_{\text{g}} + \sum_{n=1}^{6} \mathbf{F}^{\text{pw}}\left(\mathbf{r}_i - \mathbf{r}_i^{W_n}\right) + \sum_{l \ne i}^{N} \mathbf{F}^{\text{pp}}(\mathbf{r}_i - \mathbf{r}_l) + \sum_{k}^{M} \mathbf{F}^{\text{pn}}(\mathbf{r}_i - \mathbf{r}_k)\right), 1 \le i \le N, \qquad [6]$$

$$\frac{\partial \mathbf{r}_k}{\partial t} = \mathbf{u} + \mu\left(\mathbf{F}^{\text{n}}_{\text{g}} + \sum_{j=1}^{6} \mathbf{F}^{\text{nw}}\left(\mathbf{r}_k - \mathbf{r}_k^{W_j}\right) + \sum_{l \ne k}^{M} \mathbf{F}^{\text{nn}}(\mathbf{r}_k - \mathbf{r}_l) + \sum_{i=1}^{N} \mathbf{F}^{\text{np}}(\mathbf{r}_k - \mathbf{r}_i) + \mathbf{F}_{\text{el}}(\mathbf{r}_k)\right), 1 \le k \le M. \qquad [7]$$

Here the local fluid velocity and pressure are given by $\mathbf{u}$ and p, respectively. The ∇ symbol represents the spatial gradient operator, and the kinematic viscosity of the solution ν is assumed to be independent of the chemical composition. D_j is the diffusivity of the chemical C_j in the solution. μ is the mobility of particles and nodes of the elastic sheets specified below.

Unless stated otherwise, we impose no-slip boundary conditions ($\mathbf{u} = 0$) at the solid walls of the chamber. We consider two different boundary conditions for the chemical concentrations C_j: (*i*) no flux at the walls, thereby preventing chemicals from penetrating the walls, and (*ii*) some of the walls are coated with enzymes catalyzing the reactions. The respective conditions at the chamber walls, with normal $\hat{n}$, are expressed as

$$-D_j \frac{\partial C_j}{\partial n} = \begin{cases} 0, & (i)\ \text{no-flux wall}, \\ \dfrac{r^{\text{enzyme}}_{\text{m, wall}} C_j}{K_M + C_j}, & (ii)\ \text{enzyme-coated wall}. \end{cases} \qquad [8]$$

Methods describes the numerical approaches used to solve this set of coupled governing equations and boundary conditions.

Results and Discussion

Fig. 1 *C–E* reveal the biomimetic behavior that emerges when a flexible, chemically active sheet interacts with chemically responsive, diffusiophertic particles in solution. The sheet specifically encompasses four claw-like protrusions (Fig. 1*B*); this architecture allows us to investigate the sheet's ability to grab the surrounding particles and determine factors that drive multiple claw-encompassing sheets to share or compete for the particles. The central region of the sheet is coated with catalase (indicated by the green nodes); the black nodes at the apexes of the four claws are taken to be heavier than the rest of the sites. These heavier feet help anchor the sheet onto the surface and thus promote interactions between this layer and the particles that sediment to the surface.

With the introduction of H_2O_2, the catalase on the sheet decomposes this reactant into the lighter products (H_2O and O_2), causing the reactant-laden fluid to rise upward and generate an inward flow (directed toward the sheet and shown with green circular lines in Fig. 1*A*). The catalase on the sheet's bottom surface also interacts with the H_2O_2, and thus generates an inward flow directly beneath the layer. This underlying, inward

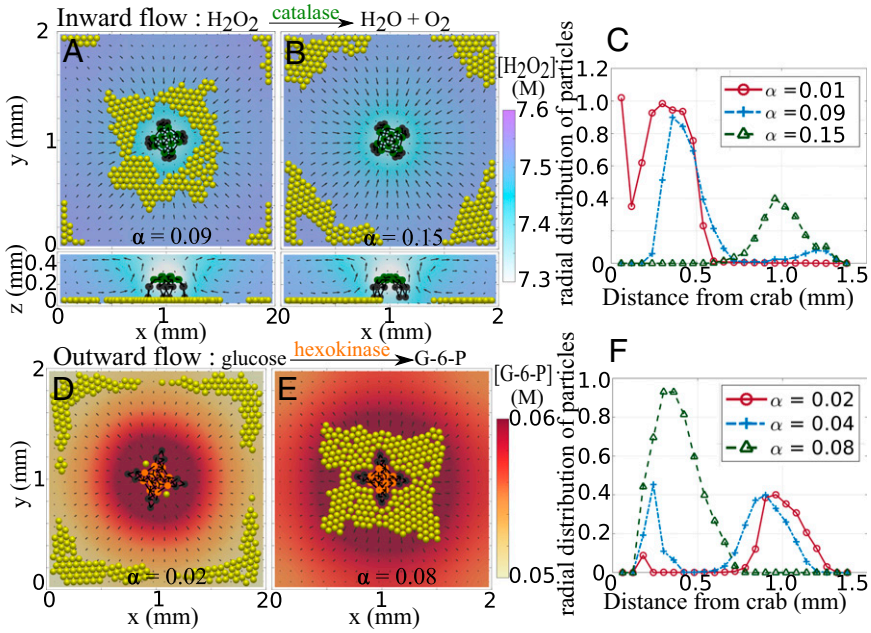

Fig. 2. Distributions of self-propelling particles around active sheets. Motility of diffusiophoretic particles and flows generated by active sheets determine how particles aggregate around sheets. (*A* and *B*) For inward flows, particle distribution pulled away from sheet with increasing α, as quantified in *C*. (*D* and *E*) For outward flows, particle distribution moves toward sheet with increasing α, as shown in *F*. The unit of α is in 10^{-10} m^5 $mol^{-1}s^{-1}$.

flow effectively pushes the center of sheet upward. The uncoated regions (gray and black sites) do not generate flow, and the heavy, black nodes keep the sheet near the surface. Consequently, the layer resembles a primitive crab whose body rises above the tips of the claws (Fig. 1*C*).

Concomitantly, the diffusiophoretic particles experience the chemical gradients, ∇C, near the bottom surface that are generated at the catalase-covered sheet and respond by moving with a velocity $\mathbf{u}_{ph} = \alpha \nabla C$, where α is the diffusiophoretic mobility and the gradient, ∇C, is computed with respect to the center of each particle. The only chemical gradient in this system is due to the local distribution of H_2O_2 in the fluid. Namely, the solutal buoyancy coefficient (β) for oxygen is sufficiently small that we neglect its contribution to the buoyancy force $\mathbf{F}_b$, and the water generated by the catalytic reaction merges with the surrounding aqueous solution. As the reaction proceeds, the sheet consumes the H_2O_2, and thus, the reactant concentration is ultimately higher away from the crab and closer to the edges of the chamber (see color bar and the side views in Fig. 1 *C*–*E* and *SI Appendix*, Fig. S1).

The distribution of particles around the crab is dictated by the competition between two opposing mechanisms. On one hand, chemical gradients near the surface drive the diffusiophoretic particles to move (with velocity $\mathbf{u}_{ph}$) away from the sheet and toward the edge of the chamber, where chemical concentration is the highest. On the other hand, the buoyancy-driven inward flow (moving with a velocity $\mathbf{u}$) drags the particles toward the sheet. In Fig. 1 *C*–*E*, the value of α is sufficiently small ($1 \times 10^{-12}\,m^5mol^{-1}s^{-1}$) that the buoyancy force dictates the behavior of the particles, which are driven toward the crab by the chemically generated inward flow (Movie S1). Thus, the sheet appears to have effectively collected and gathered all these species, much as if it were exhibiting feeding behavior.

An increase in α increases the particle velocity due to diffusiophoresis, $\mathbf{u}_{ph}$, and hence, at sufficiently high values of α, the particles move away from the sheet (Fig. 2 *A* and *B*). Fig. 2*C* shows the time-averaged radial distribution function of the particles with respect to the center of the sheet and quantifies the shift in the particle concentration away from the center of the crab as α is increased. (The nonmonotonic behavior near the center of the sheet is due to the steric repulsion between the particles and region between the claws.) Visually, the particles appear to be fleeing from the catalase-coated, green sheets.

A similar competition between the diffusiophoretic self-propulsion and the drag from the buoyancy-driven fluid also acts on the particles when the reaction generates a product that is denser than the reactant, as in the case where the catalyst hexokinase (HK) converts glucose into glucose-6-phosphate (G-6-P). Now the buoyancy mechanism drives the flow outward (away from the enzyme-coated sheet) and, for sufficiently low values of α, pushes the particles to the edge of the chamber (Fig. 2*D*). As the reactant is consumed, the concentration of product (G-6-P) is highest around the active sheet and decreases toward the edges of the box. Hence, the diffusiophoretic mechanism dictates that the particles move toward the sheet and is seen to dominate for relatively large values of α (Fig. 2*E*). This behavior is also apparent from the plot in Fig. 2*F*. (The ability of the sheets to attract or repel the diffusiophoretic particles is analyzed in more detail in *SI Appendix*.)

With two sheets in the microchamber, we can examine factors that contribute to potential competition between the crabs. The rate of reaction is a dominant factor in the overall performance of a catalyst-coated layer because a higher reaction rate leads to a faster turnover of reactants to products and, thus, can accelerate the beneficial effects of the coating. Recall that the net reaction rate *SK* ($mols^{-1}$) of an enzyme-coated object depends on the product of *S*, the surface area of the catalytic domain, and *K* ($mols^{-1}m^{-2}$), the reaction rate per unit area. To assess the influence of the product *SK*, we create a large crab with twice as many nodes as the small one and thereby double the surface area of the catalytic domain. We focus on the catalytic decomposition of H_2O_2 and fix the value of α for the diffusiophoretic particles at $2 \times 10^{-12}m^5mol^{-1}s^{-1}$. Initially, these particles are randomly and uniformly dispersed in the simulation box. (The centers' of the crabs are held fixed, restricting their lateral movement within the chamber.)

When both the large and smaller crabs (with respective net reaction rates of 2*SK* and *SK*) are placed in the same chamber, the solution in Fig. 3*A* shows a relatively low concentration of H_2O_2 around the larger crab. The faster turnover rate for the sheet with the twofold increase in the surface area of catalase produces a more rapid decomposition of the reactant. (For all of the images in Fig. 3, the sheet with the higher reaction rate is decorated in red.) Notably, the increase in the overall reaction rate generates a faster and broader inward flow around the larger sheet (as indicated by the black arrows), which is more effective at capturing the available particles than the smaller one (Fig. 3*A* and Movie S2).

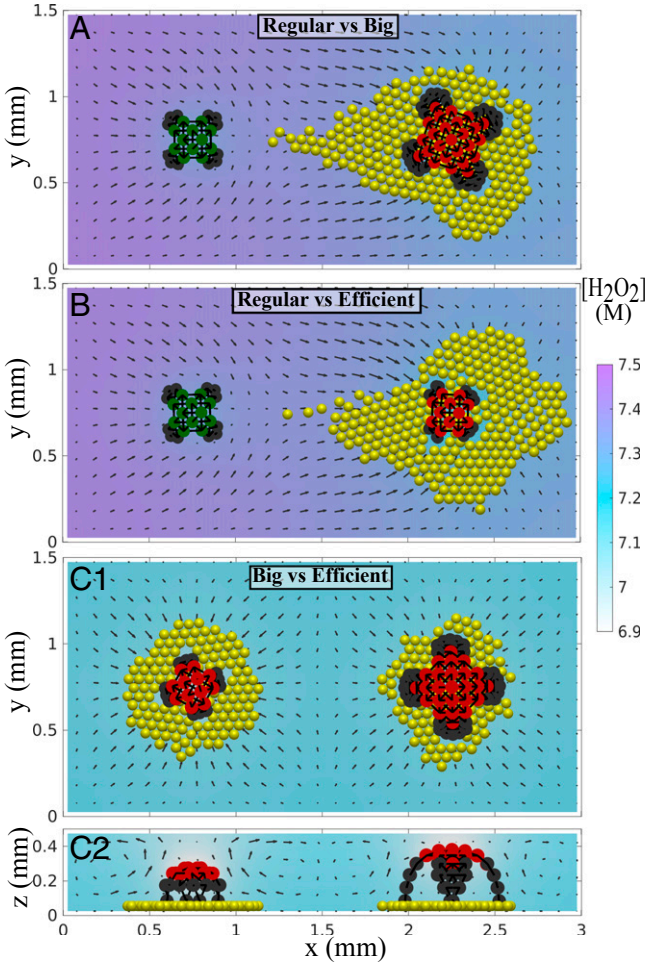

Fig. 3. Competition and sharing between two active sheets. The reaction rate is $r^{cat}_{m,sheet} = 2 \times 10^{-3}$ mol m^{-2} s^{-1} for green crabs, and $\alpha = 2 \times 10^{-12} m^5 mol^{-1} s^{-1}$. (*A*) Surface area of active sites, S, on red crab is twice that of green crab; reaction rate per node, K, is same for both. (*B*) Reaction rate per node, K, on red crab is twice that for green crab; S is same on both. Red sheets (having higher rates of decomposition) draw particles away from green competitors by generating stronger inward flows (marked with black arrows). (*C1*) Top view of winners of (*A* and *B*), whose rates of decomposition are equal, generate comparable flows, and thus gather an equal number of particles. (*C2*) Side view of case in *C1*.

Alternatively, the reaction rate for a small sheet can be increased by doubling the value of K, the reaction rate at each node. In Fig. 3*B*, the crabs have the same size (with the same coated area S), but the reaction rate for the red one is proportional to $2K$. As can be seen, the latter sheet (with the overall reaction rate of $2SK$) is more efficient than the green one (with the net reaction rate SK) since it effectively seizes all of the particles. Notably, the red sheets in Fig. 3 *A* and *B* (both having the overall reaction rate $2SK$) display very similar behavior: the species with the higher reaction rate takes all.

In the final comparison, the winners from the above contests are placed in the same microchamber (Fig. 3*C* and Movie S3). Since the rates of reaction for both crabs are $\sim 2SK$, the solution displays a spatially uniform concentration of reactants. Moreover, the black arrows point equally toward both crabs, and the magnitudes of the arrows around each crab are comparable in value. Consequently, the number of particles are equally divided between the two sheets. The side view (Fig. 3*C2*) shows that the larger crab extends further upward in the vertical direction, and hence, a greater number of particles can localize directly underneath this sheet than the smaller one, which has shorter claws and does not attain the same height.

While images in Fig. 3 show competitive activity, Fig. 4 (and Movie S4) highlights cooperative behavior among identical, mobile crabs. The crabs' motion is governed by Eqs. **3**–**7**, and our numerical approach (*Methods*) captures the fluid–structure interactions between the mobile objects and flowing fluids. Each small, catalase-coated crab is identical to the sample in Fig. 1*B*, but here $\alpha = 2 \times 10^{-12} \mathrm{m^5 mol^{-1} s^{-1}}$. Initially, in the four-crab scenario, (Fig. 4*A*), the sheets are well separated from each other (i.e., the centers of the crabs are located at 1.2 mm from each other), and the particles are uniformly dispersed in the fluid. When H_2O_2 is added to the solution, the catalase begins to decompose this reactant, and each crab generates an inward flow about its own location. At this value of α, the diffusiophoretic particles move away from each sheet (Fig. 4*B* and *SI Appendix*, Fig. S2). Eventually, however, the inward flow generated by each individual sheet brings the four close together and thereby amplifies the net flow produced by the entire group (note the increasing size of the black arrows going from Fig. 4 *A*–*C*). Ultimately, the net flow pushes the four crabs even closer together (Fig. 4*C*). Simultaneously, the increase in the flow speed and shift of the flow profile toward the center of the domain give rise to fluid flows that dominate the diffusiophoretic self-propulsion of the particles, and hence, the flow drives the particles to aggregate in the central region. In essence, the collective behavior of the four active sheets allows the community to perform a task that a single member alone could not achieve: effectively gathering all of the particles in the solution.

Another form of cooperation involves a time-dependent sharing, where one sheet localizes the particles for a finite time and then gives them to another sheet. (Alternatively, this can be viewed as competition, where one crab eventually seizes all of the particles.) This behavior is shown in Fig. 5 and Movie S5 with two crabs whose centers are held fixed, restricting their lateral movements; the green crab (left) is coated with catalase, and the pink crab (right) is coated with glucose oxidase (GOx). This system takes advantage of a cascade of chemical reactions: when glucose is added to the solution, GOx decomposes this reactant into the lighter H_2O_2 and gluconic acid. The H_2O_2 is the reactant for the catalase-coated crab, and hence, when the product of the first reaction reaches the catalase-coated crab, it initiates the second reaction. [The reaction rate for catalase is higher than that for GOx; therefore, to increase the net rate of consumption of glucose, the top wall of the chamber is also coated with GOx (4).]

Fig. 5 displays the effects of this staged process when diffusiophoretic particles are dispersed in the solution, starting with Fig. 5*A* where glucose was added into the solution. The conversion of reactants into the lighter products at the GOx-coated sheet generates an inward flow, which draws the particles toward the pink crab (Fig. 5*B*). The self-propulsion of the particles in the gradient of H_2O_2 also contributes to their movement. (Here the value of α is set to $1 \times 10^{-12} \mathrm{m^5 mol^{-1} s^{-1}}$.) As glucose is consumed, the resultant H_2O_2 activates the catalase-coated sheet and generates an inward flow; the black arrows in Fig. 5*C* clearly show that the flow is now directed toward the green crab on the left. Ultimately, this incipient flow becomes even stronger and effectively draws all of the particles away from the GOx-coated sheet, which has exhausted its reactants.

The side views in Fig. 5 reveal the complementary, synergistic behavior that allows the active crab to spatially trap the responsive particles. Namely, the chemically generated flows push the body of the more chemically active crab upward, allowing particles to occupy the space beneath this sheet. This is apparent in the significant distortion of the active crabs in Fig. 5 *B* and *C*.

The example in Fig. 5 demonstrates how cascade reactions can be harnessed to shuttle chemoresponsive particles between different active centers. By expanding the number of interrelated reactions in the cascade and adding the corresponding active sheets, the particles could be autonomously trafficked to specific locations at specified time intervals.

Conclusions

In summary, the integration of two different mechanisms for propelling the motion of particulates in solution produced new,

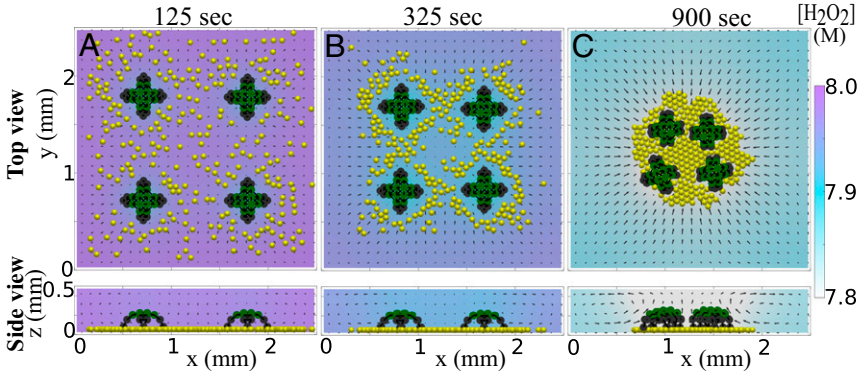

Fig. 4. Collaboration among active sheets to capture particles. (*A*–*C*) Snapshots from simulations demonstrate that catalase-coated, movable sheets acting together can capture particles that individual sheets alone cannot. Inward fluid flows become stronger (indicated by larger arrow sizes) as sheets aggregate. Reaction rate on each sheet is $r^{cat}_{m,sheet} = 1 \times 10^{-3}$ mol m^{-2} s^{-1}, and $\alpha = 2 \times 10^{-12} \mathrm{m^5 mol^{-1} s^{-1}}$.

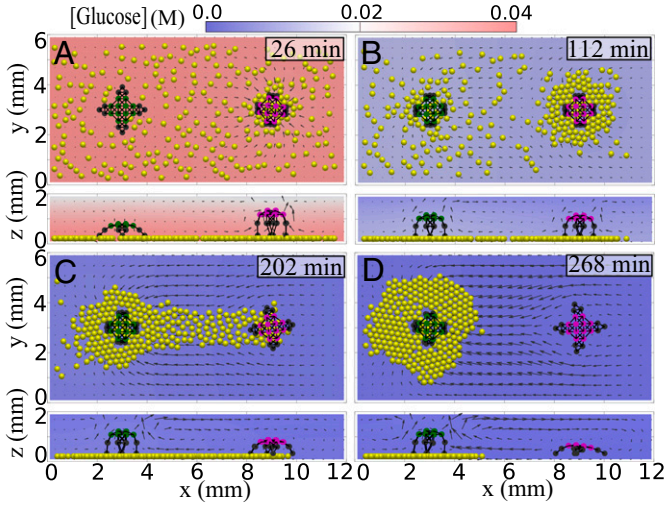

Fig. 5. Time-dependent sharing of particles by two active sheets. (*A* and *B*) GOx-coated sheet (in pink) decomposes glucose into lighter products, H_2O_2 and gluconic acid. Resulting inward flows drag particles toward pink sheet. (*C* and *D*) Eventually, catalase-coated sheet (in green) decomposes H_2O_2, generating strong inward fluid flow that drags all of the particles toward green one. In the side views, the pink sheet gradually flattens out as glucose is depleted. Reaction rates are $r^{cat}_{m,\,sheet} = 6 \times 10^{-4}$ mol m^{-2} s^{-1} and $r^{gox}_{m,\,sheet} = 2.67 \times 10^{-5}$ mol m^{-2} s^{-1};$\alpha = 1 \times 10^{-12}$m^{5}mol^{-1}s^{-1}.

synergistic interactions among all of the components. Here the solutal buoyancy mechanism that drove the motion of the fluid also gave rise to the diffusiophoresis that subsequently drove the movement of the particles. The resulting coupling between fluid-driven sheets and self-propelled particles enabled the system to display attributes that resemble biological behavior. For a single sheet with crab-like claws, the claws can either catch the particles or the particles can appear to flee the crab; this biomimetic behavior can be tailored by altering the relative influence of the mechanisms acting on the particles. For instance, increasing the height of the microchambers increases the effect of the solutal buoyancy, while decreasing this height enhances the effect of diffusiophoresis.

With more than one sheet in the solution, the system displays collaborative behavior where four interacting crabs can gather more particles than a single crab acting alone. The introduction of cascade reactions (where the product of one reaction serves as the reactant for another) permits multiple crabs to controllably transport particles to specified locations for specific periods of time (as dictated by the rate of reaction). Ultimately, this level of spatial and temporal control over the components enables the chamber to be used as a microfoundry, providing new routes for microscale fabrication.

The routes to experimentally realizing these systems are currently available. For instance, the active sheets could be fashioned from thin and flexible ribbons of chemically interlinked nanoparticles (12), which could catalyze the reactions; for example, a sheet of platinum particles could be used to catalyze the decomposition of H_2O_2. Importantly, experimental studies have shown that platinum particles are effective at driving fluid motion via solutal buoyancy (13). Alternatively, the ribbons of particles can be coated with enzymes (or other catalysts) that produce solutal buoyancy flows in the presence of the appropriate reactants. Experiments on patches of enzymes immobilized on the surface of fluid-filled microchambers provide possible candidates that can be used for these purposes (6, 8, 14). Moreover, there is a range of active particles that undergo diffusiophoretic motion in the chemical solutions considered here (15) and thus could serve as the food particles in these studies.

Methods

Eqs. **3**–**7**, along with the corresponding boundary conditions (Eq. **8**), are solved numerically within a 3D rectangular domain using a combination of the lattice Boltzmann method (16) for the fluid dynamics, the finite difference technique for the reaction–diffusion equations, and the immersed boundary (IB) approach for the fluid–structure interactions (10, 17) between the immersed objects and the flowing fluid. In the IB method, each mobile particle or discretized node in the sheet is treated as a sphere with an effective hydrodynamic radius a that experiences a fluid drag characterized by the mobility $\mu = (6\pi\rho_0\nu a)^{-1}$. As a result, the effective thickness of a single-layer elastic sheet is equivalent to the hydrodynamic diameter $2a$ of a single node. The forces $\mathbf{F}_{el}$ exerted by the nodes of the elastic sheet on the fluid calculated via the IB method (10, 17) provide zero fluid velocities at the discretization nodes of the elastic sheets and, therefore, approximate the no-slip condition for the fluid velocity, as well as no fluid permeation through the discretized boundaries of the sheets.

In Figs. 1–4, the lattice spacing in the discretized grid forming the simulation box corresponds to $\Delta x = 50$ μm; the diameter of the self-propelling particles corresponds to 60 μm, and the dimensions of the sheets are 0.675 mm × 0.15 mm. In Fig. 5, Δx is set to 200 μm to simulate a larger domain; the diameters of the particles are 0.24 mm, and dimensions of the sheets are 2.7 mm × 0.6 mm.

Values used for the Michaelis constant K_m and the maximum reaction rate r_{max} are $K_m = 0.093$ M and $r^{cat}_{max} = 0.0086$ mol m^{-2} s^{-1} for catalase (18, 19), $K_m = 0.03$ M and $r^{gox}_{max} = 2.6 \times 10^{-5}$ mol m^{-2} s^{-1} for GOx (20), and $K_m = 3 \times 10^{-4} M$ and $r^{hk}_{max} = 2.3 \times 10^{-6}$ mol m^{-2} s^{-1} for hexokinase (21).

ACKNOWLEDGMENTS. A.C.B. gratefully acknowledges funding from NSF Grant 1740630, Centers for Chemical Innovation Phase I, Center for Chemomechanical Assembly and computational facilities at the Center for Research Computing at the University of Pittsburgh. A.C.B. also acknowledges helpful discussions with Prof. S. Stupp.

1. Snezhko A, Aranson IS (2011) Magnetic manipulation of self-assembled colloidal asters. *Nat Mater* 10:698–703.
2. Palacci J, Sacanna S, Steinberg AP, Pine DJ, Chaikin PM (2013) Living crystals of light-activated colloidal surfers. *Science* 339:936–940.
3. Hay ME (2009) Marine chemical ecology: Chemical signals and cues structure marine populations, communities, and ecosystems. *Annu Rev Mar Sci* 1:193–212.
4. Laskar A, Shklyaev OE, Balazs AC (2018) Designing self-propelled, chemically active sheets: Wrappers, flappers, and creepers. *Sci Adv* 4:eaav1745.
5. Anderson JL, Prieve DC (1991) Diffusiophoresis caused by gradients of strongly adsorbing solutes. *Langmuir* 7:403–406.
6. Sengupta S, et al. (2014) Self-powered enzyme micropumps. *Nat Chem* 6:415–422.
7. Shklyaev OE, Shum H, Yashin VV, Balazs AC (2017) Convective self-sustained motion in mixtures of chemically active and passive particles. *Langmuir* 33:7873–7880.
8. Ortiz-Rivera I, Shum H, Agrawal A, Sen A, Balazs AC (2016) Convective flow reversal in self-powered enzyme micropumps. *Proc Natl Acad Sci USA* 113:2585–2590.
9. Valdez L, Shum H, Ortiz-Rivera I, Balazs AC, Sen A (2017) Solutal and thermal buoyancy effects in self-powered phosphatase micropumps. *Soft Matter* 13:2800–2807.
10. Lim S, Ferent A, Wang XS, Peskin CS (2008) Dynamics of a closed rod with twist and bend in fluid. *SIAM J Sci Comput* 31:273–302.
11. Chandrasekhar S (1961) *Hydrodynamic and Hydromagnetic Stability*, eds Marshall W, Wilkinson DH (Clarendon Press, Oxford).
12. Lee DY, et al. (2013) Macroscopic nanoparticle ribbons and fabrics. *Adv Mater* 25:1248–1253.
13. Gregory DA, Ebbens SJ (2018) Symmetrical catalytically active colloids collectively induce convective flow. *Langmuir* 34:4307–4313.
14. Zhao X, Gentile K, Mohajerani F, Sen A (2018) Powering motion with enzymes. *Acc Chem Res* 51:2373–2381.
15. Velegol D, Garg A, Guha R, Kar A, Kumar M (2016) Origins of concentration gradients for diffusiophoresis. *Soft Matter* 12:4686–4703.
16. Guo Z, Zheng C, Shi B (2002) Discrete lattice effects on the forcing term in the lattice Boltzmann method. *Phys Rev E Stat Nonlin Soft Matter Phys* 65:046308.
17. Shum H, Tripathi A, Yeomans JM, Balazs AC (2013) Active ciliated surfaces expel model swimmers. *Langmuir* 29:12770–12776.
18. Switala J, Loewen PC (2002) Diversity of properties among catalases. *Arch Biochem Biophys* 401:145–154.
19. Gaetani GF, et al. (1996) Predominant role of catalase in the disposal of hydrogen peroxide within human erythrocytes. *Blood* 87:1595–1599.
20. Raba J, Mottola HA (1995) Glucose oxidase as an analytical reagent. *Crit Rev Anal Chem* 25:1–42.
21. Recht MI, et al. (2009) Measurement of enzyme kinetics and inhibitor constants using enthalpy arrays. *Anal Biochem* 388:204–212.